ChemistrySelect

Research Article
doi.org/10.1002/slct.202400310

Chemistry Europe
European Chemical Societies Publishing

www.chemistryselect.org

Zn-Phenanthroline-Dicarboxylate Complex: A Dual Inhibitor of COX-2 and 5-LOX Enzymes

Darsi Rambabu[+],[a] Shilpa Sharma[+],[b] Mayank,[c] Narinder Singh,[b] Shagun,[d] and Pooja*[e]

A series of new phenanthroline-based metal complexes, coordination polymers are synthesized using 1,10-phenanthroline 2,9-dicarboxylate (PDA) and different metal salts including tin (**R-1** to **R-3**), manganese (**R-4**), ruthenium (**R-5**), and zinc (**R-6**) respectively. The inhibitory activities of synthesized coordination compounds are evaluated towards COX-2 (cyclooxygenase-2) and 5-LOX (5-lipoxygenase) enzymes. Among all the metal-organic coordination complexes, Zn-PDA (**R-6**) shows most prominent inhibitory activity than other systems with the IC_{50} value of 0.0524 μg/mL and 0.834 μg/mL for both COX-2 and 5-LOX enzymes, respectively. The synthesized systems were also evaluated for their activity against COX-1 and standard COX-2 inhibitors *viz.* Rofecoxib and Aspirin. The rationale for **R-6** being the most potent metal complex for dual COX-2 and 5-LOX inhibition is demonstrated using docking studies.

Introduction

The toxicity of Nonsteroidal Anti-inflammatory drugs (NSAIDs) resulted the emergence of selective cyclooxygenase-2 (COX-2) inhibitors named coxcibs.[1] However, up-regulation of 5-lipoxygenase (5-LOX) pathway through selective COX-2 inhibitors rationalized the development of new dual COX-2 and 5-LOX inhibitors.[2,3] In addition, the dual COX-2 and 5-LOX inhibitors have been found considerable in mitigating diseases like cancer and neurogenerative disorders.[4]

Metal complexes have emerged as versatile tools in medicine,[5] showcasing a wide array of applications beyond traditional drug development.[6–11] These complexes play pivotal roles in diagnostics,[7] imaging,[12] and drug delivery systems,[13] offering precise and efficient means of disease detection and treatment. In the realm of therapeutics, metal complexes exhibit promising potential as novel treatments for a range of diseases, including cancer and neurodegenerative disorders.[7–11] Further, metal complexes prepared from NSAIDs ligands have demonstrated better therapeutic potency as compared to free NSAIDs.[6] Due to the different oxidation states, charges, and spatial coordination, the structure of these metal complexes can be fine-tuned for specific targets and therapy.[7–11]

Thus, in the present manuscript, we are reporting six metal complexes synthesized using 1,10-phenanthroline-2,9-dicarboxylate (PDA) as a ligand with four different metal salts *viz.* Tin, Manganese, Ruthenium, and Zinc. The rationale to use 1,10-phenanthroline-2,9-dicarboxylate as ligand lies in the fact that it has been reported to exhibit various biological activities such as antitumor, antimicrobial and antiproliferative.[12,14–18] All metal complexes were evaluated for anti- COX-2 and 5-LOX activities. The results revealed that the Zn-based metal-organic compound (**R-6**) showed the most promising outcome as dual COX-2 and 5-LOX inhibitor. The action of the dual inhibition of the COX-2 and 5-LOX activities pathways are studied using molecular docking simulation study.

Results and Discussion

Synthesis and characterization of R-1 to R-6: The metal complexes **R-1**, **R-2**, **R-4**, **R-5**, and **R-6** were synthesized hydrothermally, however **R-3** was synthesized by mixing Sn salt and H_2PDA in DMSO (Scheme S1, ESI). The separated crystals from the reaction mixture of all compounds were characterized by single-crystal X-ray analysis. Crystal data and structure refinement parameters are given in Table S1 (see ESI)

Crystal description of R-1: Metal complex **R-1** ($C_{32}H_{28}N_4O_{10}Sn_2$) {$[Sn(CH_3)_2(PDA^{2-})]_2$ $2H_2O$} crystallizes in triclinic *P-1* space group.). The asymmetric unit of **R-1** contains one $[Sn(CH_3)]^{2+}$, one PDA^{2-} unit, and one H_2O molecule as shown in Figure 1 & S1A (ESI). The two Sn1 centers are connected through a pair of bridging oxygens (O3 and O3 from two PDA^{2-}) forming a four membered ring and resulting in a dinuclear complex. The Sn1 centers containing Sn^{4+} charge was

[a] *Dr. D. Rambabu[+]*
Institute of Condensed Matter and Nanosciences
Université catholique de Louvain
Ottignies-Louvain-la-Neuve, 1348 Louvain-la-Neuve, Belgium

[b] *Dr. S. Sharma,[+] Prof. N. Singh*
Department of Chemistry
Indian Institute of Technology Ropar
Rupnagar-140001, India

[c] *Dr. Mayank*
University College of Pharmacy
Guru Kashi University,
Talwandi Sabo-151302, India

[d] *Shagun*
School of Chemical Sciences
Indian Institute of Technology Mandi
Mandi-175001, India

[e] *Dr. Pooja*
Post Graduate Department of Chemistry
DAV College Jalandhar, Punjab-144008
E-mail: pooja02_dhir@yahoo.com

[+] *Author a & b share the same contribution.*

Supporting information for this article is available on the WWW under https://doi.org/10.1002/slct.202400310

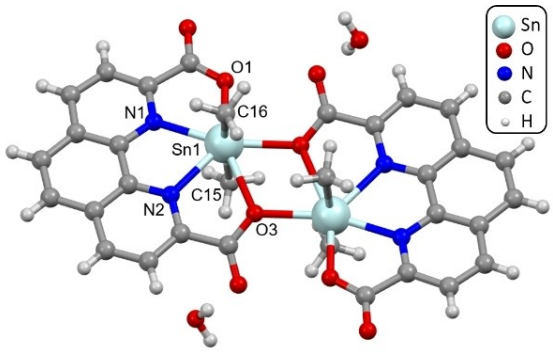

Figure 1. Dinuclear Sn complex of **R-1** with solvent water molecule.

balanced by two CH_3^- and one PDA^{2-}. The dinuclear complex of **R-1** is extended to the 1D assembly by four H-bonding interactions via O···H–O–H···O between carboxylate oxygens of PDA^{2-} and H_2O molecules (O4, O5W, Figure S1B). The dinuclear Sn complex are arranged laterally in a 1D assembly further extended into 3-D assembly by weak pi(PDA^{2-})···pi(PDA^{2-}) and C–H(methyl)···pi(PDA^{2-}) interactions (Figure S1C, ESI).

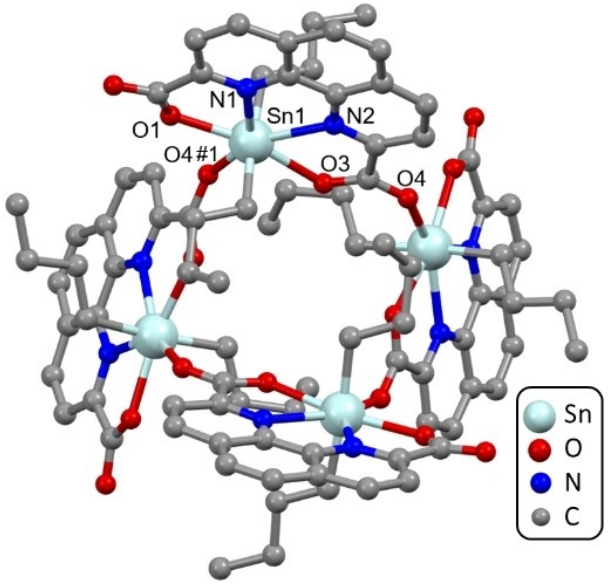

Figure 2. Crystal structure (tetranuclear Sn complex) of **R-2** (H-atoms omitted for clarity).

Crystal description of R-2: The **R-2** ($C_{88}H_{96}N_8O_{16}Sn_4$) {[Sn(n-Bu)$_2$($PDA^{2-}$)]$_4$} crystallizes in tetragonal *I-4* space group. The crystal structure is shown in Figure 2. The asymmetric unit of **R-2** contains one $[Sn(n\text{-}Bu)_2]^{2+}$ (n-Bu = n-butyl) and one PDA^{2-} ligand as shown in Figure S2A, ESI. Each Sn1 center is coordinated to O1, N1, N2, and O3 atoms (from one PDA^{2-}), O4#1 (from another PDA^{2-}) and two n-Bu groups exhibiting seven coordination numbers as shown in Figure S2B, ESI. The PDA^{2-} units are chelating to Sn1 centers five-member rings through O1, N1, N2, and O3 resulting in a mononuclear Sn complex as shown in Figure S2A and S2B, ESI. The mononuclear Sn unit is further extended to the tetranuclear Sn complex through O4, O4#1 oxygens. The PDA^{2-} units in **R-2** are arranged in alternative up and down fashion as shown in Figure S2B & S2C, ESI. The tetranuclear Sn complex of **R-2** is self-assembled with neighboring units through weak pi(PDA^{2-})···pi(PDA^{2-}) and C–H(n-Bu)···pi(PDA^{2-}) interactions (Figure S2C, ESI), forming a 3-D assembly.

Crystal description of R-3: The **R-3** ($C_{38}H_{60}N_2O_4Sn_2$) {[Sn(n-Bu)$_3$]$_2$(PDA^{2-})$_4$} crystallizes in the monoclinic *P21/n* space group (Figure 3A). The asymmetric unit of **R-3** contains two $[Sn(n\text{-}Bu)_3]^+$ (n-Bu = n-butyl), one PDA^{2-} ligand as shown in Figure S3A, ESI. **R-3** structure contains two different metal centers (Sn1 and Sn2), the Sn1 centers are coordinated to O1, N1, N2, O3 atoms (from one PDA^{2-}) and three n-Bu groups exhibiting seven coordination numbers as shown in Figure S3A and S3B, ESI. The PDA^{2-} units are chelated to Sn1 centers through O1, N1, N2, O3 and resulting in a mononuclear Sn complex shown in Figure S3B, ESI. The Sn2 centers are coordinated to O2 (from one PDA^{2-}), O4 (from another PDA^{2-}), and three n-Bu groups (Figure S3A, ESI). The Sn1 and Sn2 centers were arranged alternately where Sn2 centers bridge with the mononuclear complex of Sn1 centers through O2, O4#1 and O4, O2#2 resulting in a 1D chain (Figure 3C, ESI). Further, 1D chains of **R-3** are self-assembled with adjacent 1D chains through weak

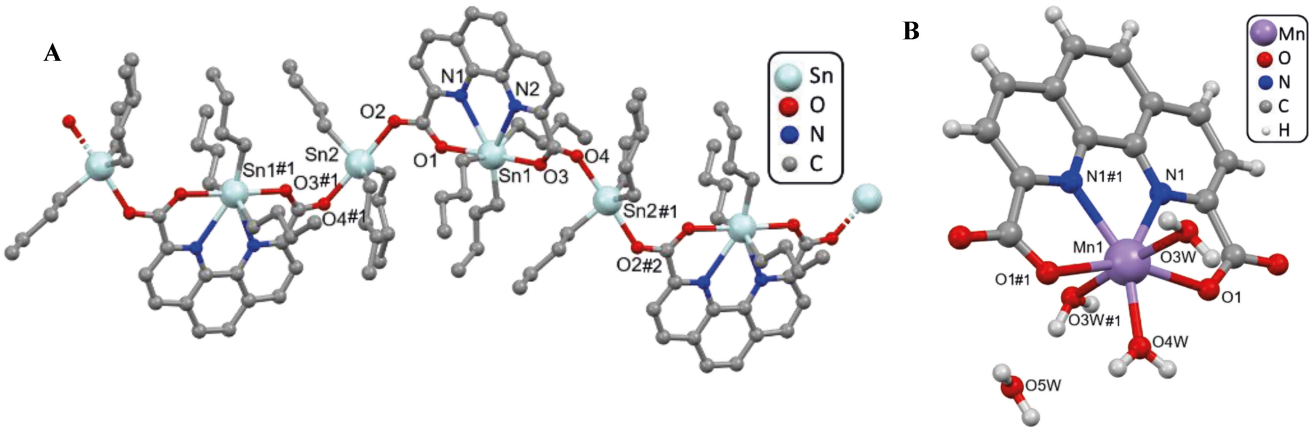

Figure 3. Crystal structure (A) (1D chain) of **R-3** (H-atoms omitted for clarity) and (B) **R-4**.

pi(PDA^{2-})···pi(PDA^{2-}) and C–H(n-Bu)···pi(PDA^{2-}) interactions forming a 3D assembly (Figure S3C, ESI).

Crystal description of R-4: The **R-4** ($C_{14}H_{16}MnN_2O_9$) {[Mn-(PDA^{2-})(H_2O)$_3$)·2H_2O} crystallizes in orthorhombic *Fddd* space group. Crystal structure is given in Figure 3B. The asymmetric unit of **R-4** contains one Mn1, one half of PDA^{2-} ligand, two H_2O molecules in which one is metal coordinated, and half of the H_2O molecule as shown in Figure S4A, ESI. The crystal structure shows Mn1 center is coordinated to O1, N1, N1#1, O1#1, atoms (from one PDA^{2-}) and three oxygen atoms O3W, O3W#1, O4W from H_2O molecules resulting in a mononuclear Mn complex as shown in Figure 3B. The PDA^{2-} units are chelated to Mn1 centers through O1, N1, N1#1, O1#1 (Figure 3B). **R-4** is extended to the 1D assembly through hydrogen bonding interactions via O–H···O between carboxylate oxygens (O1, O2) of PDA^{2-} and water molecules (O3W, O4W, and O5W) (Figure S4B and S4C, ESI). The **R-4** is further self-assembled through weak pi(PDA^{2-})···pi(PDA^{2-})interactions generating a 3D assembly (Figure S4C, ESI).

Crystal description of R-5: The **R-5** ($C_{28}H_{14}N_4O_8Ru$) {Ru(H-PDA^{-})$_2$} crystallizes in the monoclinic *P2/n* space group. The crystal structure is given in Figure 4. The asymmetric unit of **R-5** contains Ru1 and one H-PDA^{-} ligand (Figure S5A, ESI). Ru1 center is coordinated to O1, O1#1, N1, N1#1, N2 and N2#1 atoms (from two H-PDA^{-}) exhibiting six coordination number and resulting in a mononuclear Ru complex as shown in Figure 4, Each H-PDA^{-} units are chelating to Ru1 through O1, N1, N2. One carboxylate group of the H-PDA^{-} is free from metal coordination and is involved in hydrogen bonding interactions. **R-5** is extended to the 1D assembly through H-bonding interactions via O–H···O between O4 and O2 of two H-PDA^{2-}carboxylate oxygens (Figure S5B & S5 C, ESI). The **R-5** is further self-assembled through weak pi(PDA^{2-})···pi-(PDA^{2-})interactions (Figure S5C, ESI).

Crystal description of R-6: R-6 ($C_{14}H_6N_2O_4Zn$) {Zn(PDA^{2-})$_2$} crystallizes in the orthorhombic *Pbcn* space group (Figure 5). The asymmetric unit contains one Zn1, one half of the PDA^{2-} ligand as shown in Figure S6A, ESI. **R-6** containing Zn1 center is coordinated to O1#2, N1, N1#1, O1#3, atoms (from three PDA^{2-}) exhibiting tetrahedral geometry. Each tetrahedral Zn1 center are surrounded to three PDA^{2-} units (Figure 5A and 5B) and these Zn1 centers are extended to a 2-D network via carboxylate oxygens (O1) of PDA^{2-} ligands along the c-axis and a-axis as shown in Figure S6B &S6C, ESI. The Zn1 center

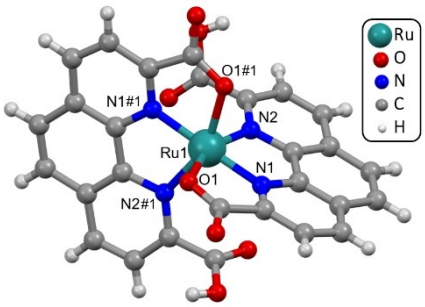

Figure 4. Crystal structure of **R-5**.

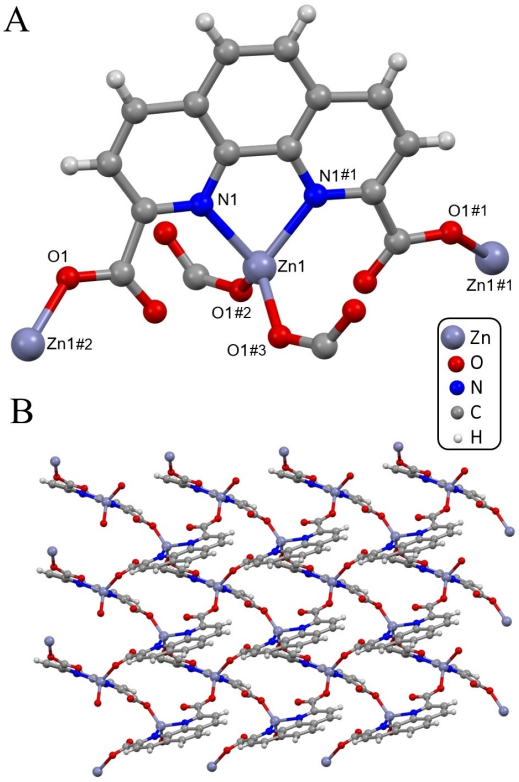

Figure 5. (A) 2-D building block of **R-6**. (B) 2-D network of **R-6** along c-axis.

containing Zn^{2+} charge is balanced by one PDA^{2-}. Further self-assembly occurs through weak pi(PDA^{2-})···pi(PDA^{2-}) interactions forming a 3D assembly (see Figure S6D, ESI).

Screening of R-1 to R-6 for Anti-Inflammatory Activity

Compounds (**R-1** to **R-6**) were examined for the inhibition of COX-1, COX-2, and 5-LOX enzymes. COX-1, COX-2, and 5-LOX enzyme immunoassays were performed as per the kit manufacturer's protocol (refer experimental section for details). We tested the compounds with a concentration of 100, 10, 1, 0.1 μg/mL for the COX-1, COX-2, and 5-LOX inhibitory activities which were quantified by measuring the amount of prostaglandins and leukotrienes, respectively during arachidonic acid (AA) metabolism produced by the enzymes in the presence of a different concentration of the metal-organic complexes. Typically, the amount of prostaglandin and leukotrienes produced by the enzyme in each well of the 96-well plate is inversely proportional to the concentration of the inhibitor (metal complexes) present therein.

We observed that the **R-6** showed excellent inhibition of COX-2 with IC_{50} of 0.0524 μg/mL, while its IC_{50} for COX-1 was 436.23 μg/mL (Table 1). The COX-2 inhibition selectivity of **R-6** is 8325 times higher with respect to COX-1 inhibition (Table 1). Complex **R-1** also showed significant inhibition activity of COX-2 and COX-1 with IC_{50} of 0.102 and 96.90 μg/mL respectively though these inhibition activities of **R-1** for COX-2 are only 950

Table 1. IC_{50} (μg/mL) values of Compounds **R-1**, **R-2**, **R-3**, **R-4**, **R-5** and **R-6** against COX-1, COX-2, and 5-LOX Enzymes.

	IC_{50} (μg/mL)			
Compound	COX-2	COX-1	Selectivity Index [a]	IC_{50} (μg/mL), LOX-5
R-1	0.102	96.90	950	4.67
R-2	3.098	44.36	14.31	76.25
R-3	4.12	135.84	32.97	45.77
R-4	0.851	153.13	179.94	37.67
R-5	8.65	68.34	7.9	158.71
R-6	0.0524	436.23	8325	0.834
NDGA	ND	ND	ND	8.2 or 27.2 μM
Phenidone	ND	ND	ND	11.1 or 68 μM
Rofecoxib	0.1 or 0.3 μM	13.2 or 42 μM	132	> 500
Aspirin	5.4 or 30 μM	0.6 or 3.5 μM	0.11	> 500

[a] IC_{50} (COX-1)/ IC_{50} (COX-2); ND = Not determined.

times higher over COX-1. **R-4** exhibited IC_{50} of 0.851 μg/mL for COX-2 and showed selectivity over COX-1, 180 times higher selectivity to COX-2 over COX-1 with IC_{50} value of 53.13 μg/mL for COX-1. In comparison to **R-6**, **R-1**, and **R-4**, showed a decent activity where as **R-2**, **R-3**, and **R-5** showed very poor inhibition activity and selectivity for COX-2 and COX-1 (Table 1). Parallel to the inhibition screening assay of COX-2, all metal complexes (**R-1**, **R-2**, **R-3**, **R-4**, **R-5**, and **R-6)** were further examined for the inhibition of 5-LOX (5-lipoxygenase). The compound **R-6** showed excellent inhibition of 5-LOX with IC_{50} of 0.834 whereas **R-1** with IC_{50} of 4.67 μg/mL showed a decent inhibiting activity. The inhibition of 5-LOX with complexes **R-2**, **R-3**, **R-4**, and **R-5** was very poor compared to **R-1** and **R-6** (Table 1).

The complexes were also compared with the standard COX-2 inhibitors and 5-LOX inhibitors under similar conditions. It was observed that in comparison to standard drugs Rofecoxib and Aspirin, selectivity of **R-1**, **R-4**, and **R-6** for COX-2 over COX-1 was far better. (Table 1). Similarly, 5-LOX inhibition activity of **R**-1 and R-6 in terms IC50 value was better than Nordihydroguaiaretic acid (NDGA) and Phenidone drugs, the standard 5-LOX inhibitors (Table 1). In addition, a comparison with ruthenium based complexes for similar biological activity is given in Table S2 of supporting information (Table S2, ESI).

Possible Mechanism of Inhibition of COX-2 and 5-LOX

Among all the metal-organic coordination compounds, **R-6** exhibited maximum inhibition of COX-2 and 5-LOX enzymes. To understand the mechanism of inhibition, we performed UV-Vis absorption titrations of **R-6** L-Glutamic acid and L-Tyrosine which are present in the active site of COX-2 (L-Tyrosine/ Tyr355/ Y355 and L-Glutamic acid/ Glu524/E524).[19,20] **R-6** (1 μg/mL) showed an increase in absorption upon addition of L-Tyrosine/L-Glutamic acid (14 μM), indicating the interaction of **R-6** with these amino acids (Figure S7, ESI).

We also conducted UV-Vis absorption titration of **R-6** with Fe(II), because of the presence of active Fe(II) center in the COX-2/5-LOX enzymes.[3,21] The increases in the absorption of **R-6** (1 μg/mL) upon addition of Fe(II) solution (14 μM) was observed as shown in Figure S8, ESI.

To confirm the selectivity of interaction of the respective enzymes with the **R-6** metal complex, **R-6** was also titrated with arachidonic acid (AA) and linolenic acid as they are present along with enzymes in the enzyme assay kit. No change in UV-Vis absorption of **R-6** on addition of arachidonic acid (AA) and linolenic acid was observed suggesting no interaction of **R-6** with arachidonic acid (AA) and linolenic acid (Figure S9, ESI).

To gain further insight, we performed its molecular docking studies. For molecular docking simulation studies, crystal structures of COX-1, COX-2, and 5-LOX were obtained from the protein data bank. In the case of COX-1 (PDBID: 2oye), a grid box of 40, 40, 40 with X, Y Z coordinates of 251, 110 and −38 respectively was created. Similarly, for COX-2 same sized box with X, Y, Z coordinates of 22, 23 and 14.139 respectively and for 5-LOX a box size of 34.224, 67.618, and 38.64 respectively was created. The binding pattern of **R-6** against COX-1, COX-2, and 5-LOX is represented in Figure 6. In the case of all three proteins, the binding cavity within the protein was found accommodating the **R-6** quite easily. Figure 6a represents the binding conformation of **R-6** against COX-1, Figure 6b represents the binding conformation against COX-2 and Figure 6c represents the binding cavity of **R-6** against 5-LOX respectively. Interactions between the metal complex and many active amino acids of the enzymes were observed. The **R-6** interacted with amino acids S530, R120, E524, S553, F518, V349, V344, W387, L531, L384, in the active site of COX-2. The interaction with E524 has also been proven with the help of UV-Vis absorption studies (Figure S7, ESI). Similarly, **R-6** interacted with amino acids *viz.* S530, A527, V350, Y355, S353, L93, R120, S87, H90, Q350, V116 in the active site of COX-1. The interactive amino acids of 5-LOX for **R-6** are R596, W599, A603, L607, H600, Q413, K409, I673, L607, W599. Thus, the binding of above-mentioned amino acids with **R-6** may have resulted in inhibition of COX-2 and 5-LOX enzymes.

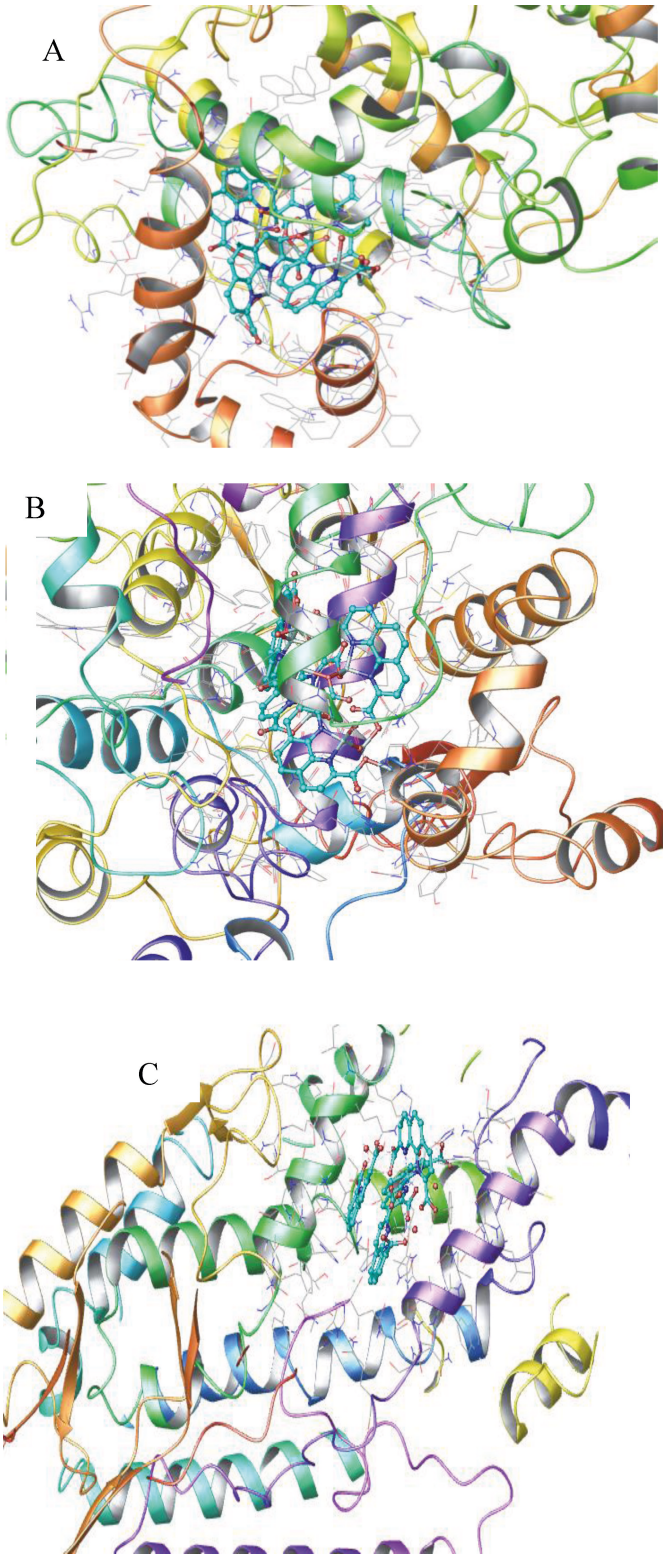

Figure 6. Molecular docking simulation pattern of **R-6** against COX-1 (A), COX-2 (B), and 5-LOX (C), showing the conformation of **R-6** inside the binding cavity of all three proteins.

Conclusions

To conclude, phenanthroline-carboxylate-based metal-organic compound **R-6** with the Zn exhibited IC_{50} value of 0.0524 μg/mL and 436.23 μg/mL against COX-2 and COX-1 enzymes respectively and showed 8325 selectivity index with respect to COX-1 inhibition. In addition, coordination polymer **R-6** exhibited appreciable inhibition of 5-LOX with IC_{50} of 0.834 μg/mL. This work may lead researchers to design more metal-organic compounds (complexes, coordination polymers and Metal-organic frameworks) as efficient dual COX-2 and 5-LOX inhibitors which can be converted to a commercial metallodrug in years to come.

Experimental Section

The PDA (1,10-phenanthroline-2,9-dicarboxylic acid) was synthesized by the previously reported procedure.[22]

1. Synthesis of R-1: A mixture of 0.075 g (0.28 mmol) of PDA (1,10-phenanthroline-2,9-dicarboxylic acid) and 0.056 g (0.28 mmol) Trimethyltin chloride $(Sn(CH_3)_3Cl)$ in 15 mL of distilled water was placed in parr's acid digestion bomb and heated in an oven at 130 °C for 24 h. The mixture was allowed to cool at room temperature for overnight to obtain yellow-coloured crystals (0.090 g, yield 74.4% with respect to PDA) which were washed with water (3×1 mL) and dried under vacuum at room temperature.

2. Synthesis of R-2: A mixture of 0.075 g (0.28 mmol) of PDA (1,10-phenanthroline-2,9-dicarboxylic acid) and 0.182 g (0.56 mmol, 0.152 mL) Tributyltin chloride $(Sn(n\text{-}Bu)_3Cl)$ (n-Bu = n-butyl) in 15 mL of distilled water was placed in parr's acid digestion bomb and heated in oven at 130 °C for 9 h. The mixture was allowed to cool at room temperature for overnight to obtain yellow-coloured crystals (0.068 g, yield 48.6% with respect to PDA) which were washed with DMSO (1×1 mL) and water (3×1 mL) and dried under vacuum at room temperature.

3. Synthesis of R-3 (mix and allow method): 0.075 g (0.28 mmol) of PDA (1,10-phenanthroline-2,9-dicarboxylic acid) and 0.250 g (0.42 mmol, 0.214 mL) of Bis(tributyltin) oxide $\{[Sn(n\text{-}Bu)_3]_2O\}$ (n-Bu = n-butyl) were dissolved separately in two different vials containing 2.5 mL DMSO. Once dissolved, immediately combined both solutions and shaken for 1 min and stand for 2 h without disturbing at room temperature (crystals were observed within 10 min). The yellow crystals of R-3 (0.190 g, yield 80.2% with respect to PDA) were filtered and dried under vacuum at room temperature.

4. Synthesis of R-4: A mixture of 0.038 g (0.14 mmol) of PDA (1,10-phenanthroline-2,9-dicarboxylic acid) and 0.053 g (0.21 mmol) of $Mn(NO_3)_2.4H_2O$ in 15 mL of distilled water and DMF (2:1 ratio) solution was placed in parr's acid digestion bomb and heated in an oven at 150 °C for 72 h. The mixture was allowed to cool at room temperature for overnight to obtain yellow coloured crystals (0.044 g, yield 76.2% with respect to PDA) which were washed with DMF (3×1 mL) and water (3×1 mL) and dried under vacuum at room temperature.

5. Synthesis of R-5: A mixture of 0.075 g (0.28 mmol) of PDA (1,10-phenanthroline-2,9-dicarboxylic acid) and 0.037 g (0.14 mmol) of $RuCl_3.3H_2O$ in 8 mL of distilled water was placed in parr's acid digestion bomb and heated in an oven at 150 °C for 72 h. The mixture was allowed to cool at room temperature for overnight to obtain red coloured crystals (0.057 g, yield 64.1% with respect to

PDA) which were washed water (3×1 mL) and dried under vacuum at room temperature.

6. Synthesis of R-6: A mixture of 0.075 g (0.28 mmol) of PDA (1,10-phenanthroline-2,9-dicarboxylic acid) and 0.125 g (0.42 mmol) of $Zn(NO_3)_2.6H_2O$ in 10 mL of distilled water was placed in parr's acid digestion bomb and heated in an oven at 150 °C for 72 h. The mixture was allowed to cool at room temperature for overnight to obtain yellow-coloured crystals (0.071 g, yield 76.3% with respect to PDA) which were washed with water (3×1 mL) and dried under vacuum at room temperature.

COX-1/COX-2 Inhibitory Activities: *In vitro* COX-1 and COX-2 inhibitory activities were evaluated using "COX inhibitor screening assay" kits with 96-well plates (catalog no. 560101, Cayman Chemical, Ann Arbor, MI) according to the manufacturer's instructions. As per the kit specifications, the enzymes were ovine COX-1 and human recombinant COX-2. This screening assay directly measures PGF2a produced by $SnCl_2$ reduction of COX-derived PGH2. COX-1 and COX-2 initial activity tubes were prepared to take 950 μL of reaction buffer (0.1 M Tris-HCl, pH 8.0, containing 5 mM EDTA and 2 mM phenol), 10 μL of heme, 10 μL of COX-1 and COX-2 enzymes into respective tubes. Similarly, COX-1 and COX-2 inhibitor tubes were prepared by adding 20 μL of inhibitor (compound of 0.1 μg/mL, 1 μg/mL, 10 μg/mL and 100 μg/mL concentrations were prepared in DMSO) in each tube in addition to the above ingredients, making a final volume of 1 mL. The background tubes correspond to inactivated COX-1 and COX-2 enzymes obtained after keeping the tubes containing enzymes in boiling water for 3 min. After incubation of the tubes at 37 °C for 20 min, reactions were initiated by adding 10 μL of arachidonic acid in each tube and again incubating at 37 °C for 2 min. The reaction was quenched with 50 μL of 1 M HCl. PGH2 thus formed was reduced to PGF2a by adding 100 μL of $SnCl_2$. The prostaglandin produced in each well was quantified using broadly specific prostaglandin antiserum. The PGs and PG acetylcholinesterase (AChe) conjugate (PG tracer) have a competition for a limited amount of PG antiserum. Because the concentration of the PG tracer is held constant while the concentration of PG varies, the amount of PG tracer that is able to bind to the PG antiserum will be inversely proportional to the concentration of PG in the well. This rabbit antiserum-P (either free or tracer) complex binds to a mouse monoclonal antirabbit antibody that has been previously attached to the well. The plate is washed to remove any unbound reagents, and then Ellman's reagent (which contains the substrate to AChe) is added to the well. The product of this enzymatic reaction has a distinct yellow colour and absorbs strongly at 420 nm. The intensity of this color, determined spectrophotometrically, is proportional to the amount of PG tracer bound to the well, which is inversely proportional to the amount of free PG present in the well during the incubation. The wells of the 96-well plate showing low absorbance at 420 nm indicate the higher level of prostaglandins in these wells and hence less inhibition of the enzyme. Therefore, the COX inhibitory activities of the compounds could be quantified from the absorbance values of different wells of the 96-well plates. The concentrations of the test compound causing 50% inhibition (IC_{50}) were determined using a dose-response inhibition curve (duplicate determinations) with GraphPad Prism.

5-LOX inhibitory activities: For 5-LOX inhibition studies, (Lipoxygenase Inhibitor Screening Assay Kit, Item No. 760700 was used from Cayman Chemicals Co.), solutions of complexesR-1, R-2, R-3, R-4, R-5 and R-6 at 0.1 μg/mL, 1 μg/mL, 10 μg/mL and 100 μg/mL concentrations were prepared in DMSO. 10 μl of each compound from the three concentrations was added to a 90 μl solution (in assay buffer) of 5-LOX enzyme taken in a 96-well plate. Each complex was tested in triplicate. Two wells were taken as blanks (assay buffer + arachidonic acid) and two wells were taken as positive controls (enzyme in assay buffer + arachidonic acid). The reaction was initiated by the addition of 10 μl of the substrate (arachidonic acid). After maintaining the 96-well plate on a shaker for 5 min, 100 μl of the chromogen (developing reagent) was added to each well. The plate was again shaken for 5 min and read at 500 nm in a microplate scanning spectrophotometer. Percent 5-LOX inhibitory activity was determined using the mean of the three values for each sample from the calculations given below:

$$\text{Lipoxygenase activity } (\mu\text{mol/min/mL}) = [A_{500}/\text{min}/9.47\ \text{mM}^{-1}] \times [0.21\ \text{mL}/0.09\ \text{mL}] \times \text{sample dilution}$$

Where $A_{500}/\text{min} = A_{500}$ (sample)/min $- A_{500}$ (blank)/5 min,

$9.47\ \text{mM}^{-1}$ = Extinction coefficient of chromogen,

0.21 mL = Total volume of the solution in each well and

0.09 mL = Volume of the enzyme solution used.

$$\text{Percent 5-LOX inhibition} = [\{\text{L.A. (P.C.)} - \text{L.A. (I.)}\}/\text{L.A. (P.C.)}] \times 100$$

L.A. (P.C.) – Lipoxygenase Activity of positive control,

L.A. (I.) – Lipoxygenase Activity of inhibitor.

IC_{50} values were determined from the graph between Percent Inhibition vs. inhibitor concentration.

Molecular docking simulation studies, Autodock software was used.[23–25] Herein, protein, preparation, ligand preparation, grid generation, and molecular docking simulation steps are executed using various tools that are available in Autodock software. During protein preparation, associated water molecules were deleted, hydrogens were added, and any co-crystallized ligand if the present was also deleted and finally gasteiger charges were added to produce the required PDBQT file. For Grid generation, Autogrid 4.2 was used, and herein, and initially the GPF and finally, the GLP was created. During molecular docking simulation studies, Autodock 4.2 was used, and herein, a genetic algorithm was selected for our studies.

Acknowledgements

Pooja is thankful to SERB for award of project SB/FT/CS-040/2013. Pooja acknowledges Dr. Abhimanew Dhir, Assistant Professor, IIT Mandi for Laboratory Infrastructural Support.

Conflict of Interests

The authors declare no conflict of interest.

Keywords: COX-2 · 5-LOX · Inhibitors · Metal Complexes · Crystal Structures

[1] J. A. Cairns, *Can. J. Cardiol.* **2007**, *23*, 125–131.
[2] D. W. Gilroy, A. Tomlinson, D. A. Willoughby, *Eur. J. Pharmacol.* **1998**, *355*, 211–217.
[3] C. Charlier, C. Michaux, *Eur. J. Med. Chem.* **2003**, *38*, 645–659.
[4] M. A. Meshram, U. O. Bhise, P. N. Makhal, V. R. Kaki, *Eur. J. Med. Chem.* **2021**, *225*, 113804.

[5] H. S. Mohammed, V. D. Tripathi, *J. Phys. Conf. Ser.* **2020**, *1664*, 012070.
[6] H. Yasir Khan, S. Parveen, I. Yousuf, S. Tabassum, F. Arjmand, *Coord. Chem. Rev.* **2022**, *453*, 214316.
[7] K. L. Haas, K. J. Franz, *Chem. Rev.* **2009**, *109*, 4921–4960.
[8] A. C. F. Santos, L. P. G. Monteiro, A. C. C. Gomes, F. Martel, T. M. Santos, B. J. M. L. Ferreira, *Int. J. Mol. Sci.* **2022**, *23*, 2855.
[9] M. Simunkova, P. Lauro, K. Jomova, L. Hudecova, M. Danko, S. Alwasel, I. M. Alhazza, S. Rajcaniova, Z. Kozovska, L. Kucerova, J. Moncol, L. Svorc, M. Valko, *J. Inorg. Biochem.* **2019**, *194*, 97–113.
[10] E. Halevas, S. Matsia, A. Hatzidimitriou, E. Geromichalou, T. A. Papadopoulos, G. Katsipis, A. Pantazaki, G. Litsardakis, A. Salifoglou, *J. Inorg. Biochem.* **2022**, *235*, 111947.
[11] R. Kumari, S. Banerjee, P. Roy, M. Nath, *Appl. Organomet. Chem.* **2020**, *34*, 1–24, DOI 10.1002/aoc.5283.
[12] M. R. Gill, J. A. Thomas, *Chem. Soc. Rev.* **2012**, *41*, 3179.
[13] D. Rambabu, P. Negi, A. Dhir, A. Gupta, Pooja, *Inorg. Chem. Commun.* **2018**, *93*, 6–9.
[14] M. M. Meier, C. Rajendran, C. Malisi, N. G. Fox, C. Xu, S. Schlee, D. P. Barondeau, B. Höcker, R. Sterner, F. M. Raushel, *J. Am. Chem. Soc.* **2013**, *135*, 11670–11677.
[15] C.-H. Leung, S. Lin, H.-J. Zhong, D.-L. Ma, *Chem. Sci.* **2015**, *6*, 871–884.
[16] I. Naletova, C. Satriano, A. Curci, N. Margiotta, G. Natile, G. Arena, D. La Mendola, V. G. Nicoletti, E. Rizzarelli, *Oncotarget* **2018**, *9*, 36289–36316.
[17] A. Hussain, M. F. AlAjmi, M. T. Rehman, S. Amir, F. M. Husain, A. Alsalme, M. A. Siddiqui, A. A. AlKhedhairy, R. A. Khan, *Sci. Rep.* **2019**, *9*, 5237.
[18] M. Porchia, M. Pellei, F. Del Bello, C. Santini, *Molecules* **2020**, *25*, 5814.
[19] H. Zhang, J. Fan, J. Wang, B. Dou, F. Zhou, J. Cao, J. Qu, Z. Cao, W. Zhao, X. Peng, *J. Am. Chem. Soc.* **2013**, *135*, 17469–17475.
[20] A. S. Kalgutkar, B. C. Crews, S. W. Rowlinson, A. B. Marnett, K. R. Kozak, R. P. Remmel, L. J. Marnett, *Proc. Nat. Acad. Sci.* **2000**, *97*, 925–930.
[21] R. Young, *Eur. J. Med. Chem.* **1999**, *34*, 671–685.
[22] C. J. Chandler, L. W. Deady, J. A. Reiss, *J. Heterocycl. Chem.* **1981**, *18*, 599–601.
[23] G. M. Morris, R. Huey, W. Lindstrom, M. F. Sanner, R. K. Belew, D. S. Goodsell, A. J. Olson, *J. Comput. Chem.* **2009**, *30*, 2785–2791.
[24] S. Cosconati, S. Forli, A. L. Perryman, R. Harris, D. S. Goodsell, A. J. Olson, *Expert Opin. Drug Discovery* **2010**, *5*, 597–607.
[25] S. Forli, A. J. Olson, *J. Med. Chem.* **2012**, *55*, 623–638.

Manuscript received: January 27, 2024